Airborne Doppler Radar Observations in Hurricane Debby

Frank D. Marks, Jr.[1] and
Robert A. Houze, Jr.[2]

Abstract

A pulse-Doppler radar on board a National Oceanic and Atmospheric Administration (NOAA) WP-3D research aircraft has been used to map the wind field in the vicinity of the developing eye wall of Hurricane Debby, which occurred in 1982. The Doppler-derived winds in the eye wall region compare favorably with winds measured aboard the aircraft. The Doppler radar allowed the wind field to be documented in much more detail than has been possible in previous hurricane studies. The maximum winds were found radially, just inward of the band of maximum radar reflectivity, and were concentrated in two mesoscale maxima. A mesoscale trough associated with the developing eye wall sloped upwind and radially outward through the 1–5 km layer. The trough was best defined at 2–3 km, where it contained a closed mesocyclonic circulation.

1. Introduction

Until recently, wind patterns in hurricane eye walls and rainbands could be obtained only by constructing composites based on measurements made along aircraft flight tracks (Shea and Gray, 1973; Barnes *et al.*, 1983; Jorgensen, 1984a,b). These composites have provided a good first approximation to eye wall and rainband circulations; however, they yield limited information on spatial and temporal variability. With the advent of pulse- Doppler radar aboard one of the National Oceanic and Atmospheric Administration's (NOAA) WP-3D aircraft (Trotter *et al.*, 1981; Jorgensen *et al.*, 1983), it has become feasible to measure the horizontal wind field with high vertical resolution throughout a large volume of space surrounding the aircraft. The first attempt to use this new technology in the study of a hurricane is described in this paper.

The Doppler radar system on the WP-3D measures the mean along-beam velocity components of echoes detected with an X-band (3 cm wavelength) radar. The radar antenna, located in the tail of the aircraft, points normally to the aircraft's ground track and sweeps circularly through elevation angles of 0–360°.[3] Observation of the same echo volume from two or more viewing angles allows the horizontal wind vector to be reconstructed using dual-Doppler radar analysis techniques.

The measurements analyzed in this study were obtained during a test of the airborne Doppler system on a flight through the inner-core region of Tropical Storm Debby of 1982 while the storm was developing to hurricane strength. Rainbands near the center of the storm were present and evolving into a more circular structure. The flow pattern at this stage of the storm could be mapped because the process of evolution was slow enough to allow the aircraft to obtain velocity component measurements from two viewing angles over a large portion of the storm before the storm's structure changed substantially.

Recent observational studies carried out without the aid of Doppler radar (Willoughby *et al.*, 1982; Barnes *et al.*, 1983; Jorgensen, 1984a,b) and recent theoretical and numerical investigations (Shapiro and Willoughby, 1982; Willoughby *et al.*, 1984) have led to useful idealizations of the radial and vertical (i.e., 2-dimensional) structures of hurricane inner-core circulation. By providing a detailed 3-dimensional field of air motions, the airborne Doppler measurements in Debby indicate a structure of the wind field not evident in these previous studies. The airborne Doppler data is used to examine the wind field for mesoscale features superimposed on the basic circulation pattern of the developing inner core of Debby. The quality of the airborne Doppler data, and their usefulness and limitations for future hurricane research, also are considered.

2. Large-scale storm structure and flight pattern

During the period of our analysis (1950–2045 GMT, 14 September 1982), Debby was located near 25°N, 69°W, and was moving toward the north-northeast at 4–5 $m \cdot s^{-1}$. The storm was increasing in intensity (it actually did not reach hurricane strength until 0000 GMT, 15 September), and an eye wall was forming. While the aircraft was in the storm, the central pressure was 995 mb and the peak wind speed encountered by the aircraft (flying at an altitude of 450 m) was 30–35 $m \cdot s^{-1}$.

Figure 1 shows the flight track (relative to the storm center) and a composite radar reflectivity pattern derived from the aircraft's C-band (5 cm wavelength) lower fuselage radar.[4] The flight track was obtained by plotting the aircraft position in a rectangular Cartesian grid with X positive to the east, Y positive to the north, and origin (point (0,0) in Fig. 1) located at the center of the storm. The storm track was determined objectively using a procedure described by Willoughby and Chelmow (1982). The time-composite reflectivity pattern was constructed by mapping each ray of data collected with

[1] Hurricane Research Division, Atlantic Oceanographic and Meteorological Laboratory, NOAA, Miami, FL 33149.
[2] Department of Atmospheric Sciences, University of Washington, Seattle, WA 98195.
[3] Other characteristics of the tail radar are given by Jorgensen (1984a).

[4] Characteristics of this radar are given by Houze *et al.* (1981).

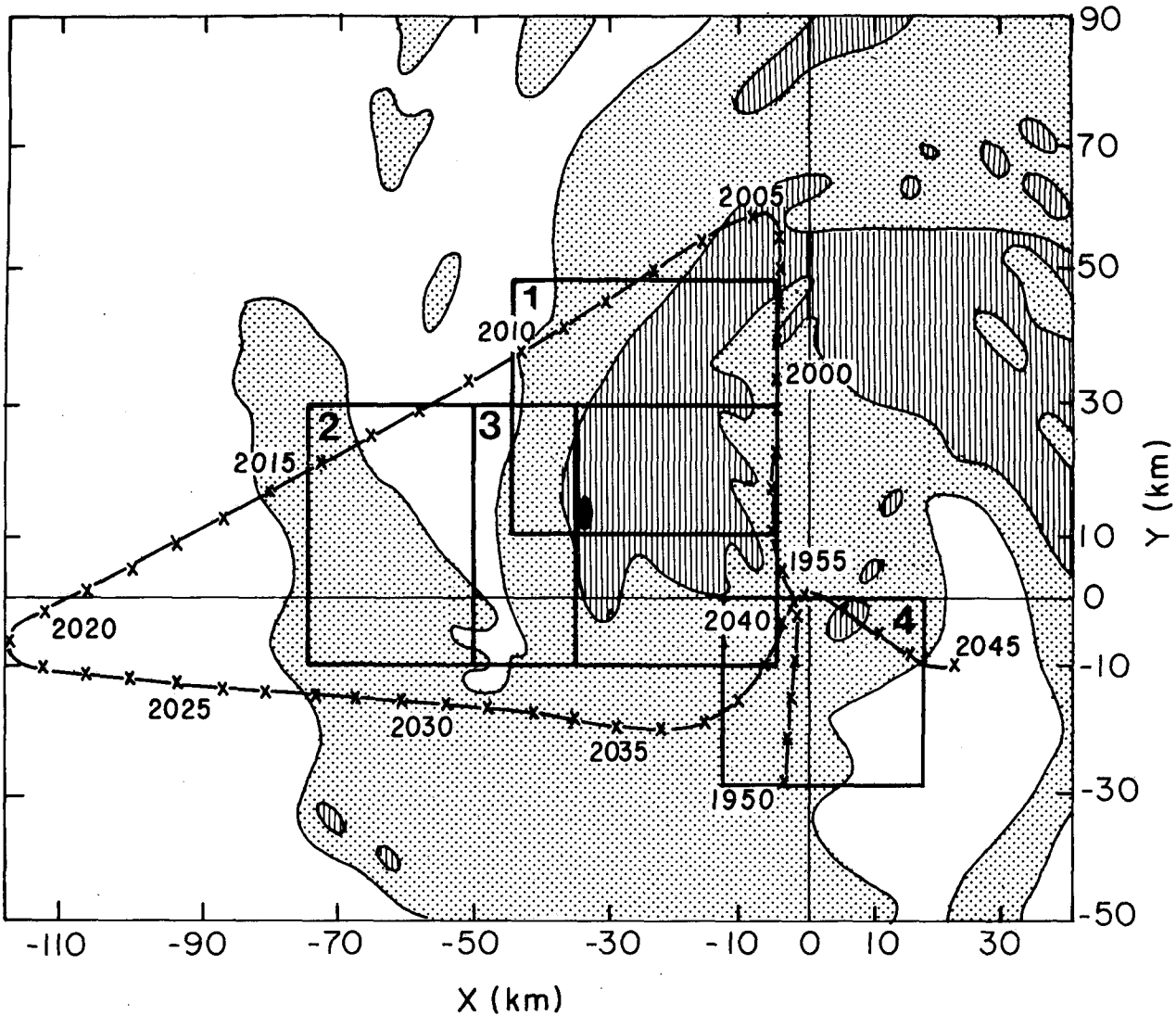

FIG. 1. Temporal composite of the horizontal distribution of reflectivity in Tropical Storm Debby for 1950–2045 GMT, 14 September 1982. The reflectivity contours are for 20, 30, and 40 dB(Z). The aircraft flight track is indicated by the thin solid line, and the analysis Boxes 1, 2, 3, and 4 are denoted by the thick solid lines. The origin of the coordinate system is located at the storm center, and the aircraft positions have been plotted relative to the storm's center. Coordinates are east-west distance, X, and north-south distance, Y, from the storm center.

the lower fuselage radar into the rectangular grid attached to the storm center. When more than one reflectivity measurement was mapped into a particular grid square, the largest value was taken to be the best estimate of the reflectivity in that grid square. This procedure minimizes the effects of attenuation and beam geometry in producing underestimates of the reflectivity.

Figure 1 shows that a symmetric eye wall was not present during the time period under consideration; however, a prominent rainband curved around the north side of the storm. Peak reflectivities in this band were 40–44 dB(Z) near the end of the band, west-northwest of the storm center. Later in the day, a portion of this rainband wrapped around the center of the storm and took on the appearance of a mature eye wall; hence, we refer to the strong curved rainband seen at the time of Fig. 1 as a "developing eye wall." An area of weak stratiform precipitation (with reflectivity below the lowest threshold shown in Fig. 1) existed to the west of the storm center, just outside the developing eye wall. A stratiform rainband was located still farther west, centered along the east-west coordinate X = −70 km. The highest reflectivities in this stratiform band were only 23–25 dB(Z).

3. Methods of analysis

Dual-Doppler analyses of the winds in Debby have been carried out for the boxes labelled 1–4 in Fig. 1. Boxes 1 and 3 cover the western portion of the developing eye wall, Box 2 covers a representative portion of the stratiform precipitation located outside the eye wall, and Box 4 covers the south-

eastern quadrant of the hurricane's inner core. Wind analysis for Box 1 was constructed from the tail radar data obtained on the north–south flight leg (1955–2004 GMT) and the northeast–southwest leg (2005–2014 GMT). An analysis for Box 2 was constructed from data obtained on the northeast–southwest flight leg and the east–west leg (2028–2035 GMT), and winds for Box 3 were determined from measurements made on the north–south and east–west legs. Box 3 had ideal viewing angles, since the legs were nearly perpendicular; however, the time elapsed between the two legs was 40–50 min. Only fairly stationary features of the field could be inferred in this region. Inclusion of this box, allowed for the analysis of the developing eye wall to be extended southward, where some particularly interesting features of the flow were located. Analyses for Box 4 were constructed from the L-shaped flight track extended from 2038 to 2043 GMT. The L was divided into nearly orthogonal legs by splitting it at 2041 GMT.

For each box, 3-dimensional time-composite reflectivity patterns were constructed by a method analogous to that used to obtain the 2-dimensional time-composite reflectivity map in Fig. 1. Each box was subdivided into grid elements 1 km × 1 km in the horizontal and 0.5 km in the vertical. While flying along the two flight legs contributing to each box, each ray of reflectivity data obtained with the tail radar was mapped into the 3-dimensional Cartesian grid contained in the box. Each datum taken from a ray was positioned at the center of the grid element into which it was mapped. When more than one reflectivity measurement was mapped into a particular grid element, the largest value was taken to be the best estimate of the reflectivity in that element.

Three-dimensional fields of horizontal wind were constructed from the rays of radial velocity data obtained with the tail radar while the aircraft was flying along the flight legs contributing to each analysis box. First, the radial velocities in each ray were examined and accepted only if the reflectivity was above a specified noise level (typically 6–10 dB(Z)). Then the accepted radial velocities in each ray were unfolded automatically using Bargen and Brown's (1980) method, with the wind at zero range being given by the wind measurement made on board the aircraft. The unfolded radial velocities were converted trigonometrically to horizontal wind components normal to the ground track of the aircraft. The horizontal wind components thus obtained for one flight leg then were mapped into the 3-dimensional Cartesian grid contained within the analysis box. When more than one horizontal velocity component was mapped into a particular grid element, the average component was computed and used as the best estimate for that grid element. This procedure was repeated for the second flight leg contributing to the analysis box. Each grid volume then contained averaged horizontal velocity components observed from zero, one, or two viewing angles. The horizonal wind vector was computed for all grid volumes containing two components. This so-called pseudo-dual Doppler analysis method is described in more detail by Jorgensen *et al.* (1983).

The fields of horizontal wind produced by this method were inspected for spurious values generated by incorrect unfolding or other problems. The data were edited manually to remove these bad points. The edited winds then were smoothed with the 2-dimensional Gaussian low-pass Shuman filter given by Eq. (A12) in Ray *et al.* (1975). This filter has responses of nearly zero, 25%, and 75% at wavelengths of 3, 4, and 8 km, respectively. This smoothing was necessary to remove the effects of transient convective wind fluctuations that may have occurred while the aircraft moved from one viewing position to the next. The times between viewing positions were: 8–15 min in Box 1, 19–25 min in Box 2, and 40–50 min in Box 3. Our smoothing seeks to retain only those features that did not change structure significantly over these time periods.

Three-dimensional fields of horizontal divergence and vorticity were computed from the final edited and smoothed winds. The grid spacing in X and Y used to compute the divergence was 2 km.

4. Data quality

The quality of the data used in this study was examined in two ways: 1) by comparing the Doppler-derived winds at the 0.5 km level with the aircraft winds measured along the flight track at an altitude of 450 m, and 2) by comparing the Doppler-derived winds in different boxes in regions where the boxes overlapped.

a. Low-level winds

Doppler-derived winds at 0.5 km are shown with the 450 m level aircraft winds in Fig. 2. The Box 1 Doppler-derived winds are shown in Fig. 2a, with Doppler winds from the southern part of Box 3 and the aircraft winds along portions of the flight track shown for comparison. The Box 1 winds are highly consistent with the aircraft winds, except in the southeastern corner of Box 1, where the aircraft winds are more easterly than the Box 1 Doppler winds. The center of cyclonic rotation was located just to the south and east of this corner of Box 1, however, and the directional change from easterly along the flight track to northeasterly just inside the corner of the box was probably a real spatial variation. The Box 1 winds also are in good agreement with the Box 3 winds. This agreement can be seen along the southern border of Box 1 in Fig. 2a and in Fig. 2b, which shows the complete Box 3 analysis. The entire northern portion of the Box 3 analysis (Y = 0–30 km) is consistent with both the winds in the corresponding region of Box 1 (Fig. 2a) and the aircraft winds to the northwest and east.

The winds in the southeastern portion of Box 3 (Fig. 2b) reflect the cyclonic circulation around the storm and generally are consistent with the aicraft winds, with two exceptions.

FIG. 2. Doppler-derived winds at 0.5 km level and 450 m level aircraft winds. The latter are plotted along flight tracks labelled at 5 min intervals (GMT). a) (*Page 572*) Doppler-derived winds in Box 1 (northern box) and Box 3 (only southern part of box is shown). b) (*Page 573*) Doppler-derived winds in Box 3. c) (*Page 574*) Doppler-derived winds in Box 2. d) (*Page 575*) Doppler-derived winds in Box 4. e) (*Page 576*) Mosaic of Doppler-derived winds in Boxes 1, 3, and 4, with streamlines and storm-center location implied by the streamlines of the Doppler winds also indicated. The wind plotting convention is: flag, 25 $m \cdot s^{-1}$; barb, 5 $m \cdot s^{-1}$; and half-barb, 2.5 $m \cdot s^{-1}$.

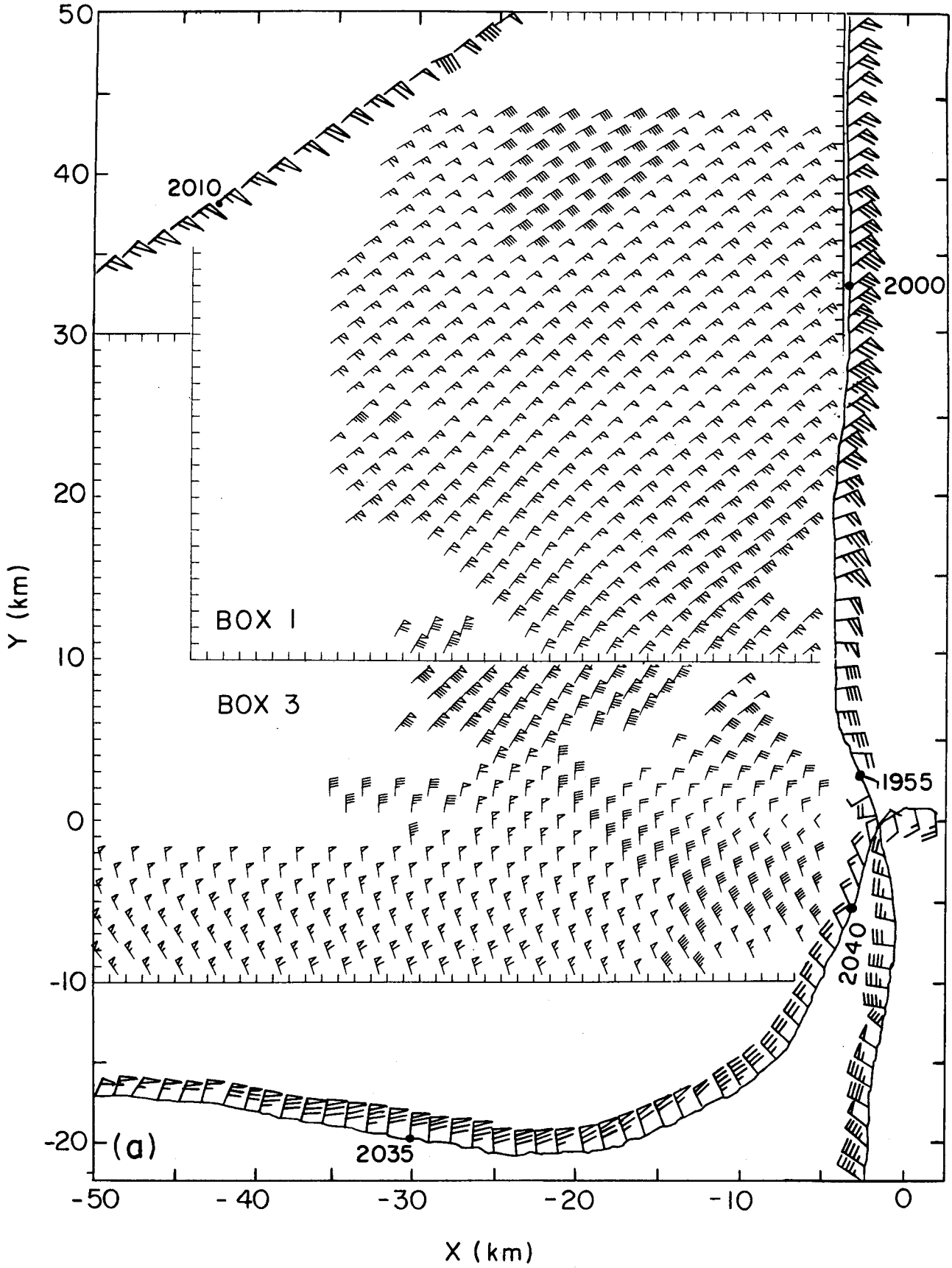

FIG. 2a. Doppler-derived winds in Box 1 (northern box) and Box 3 (only southern part of box is shown).

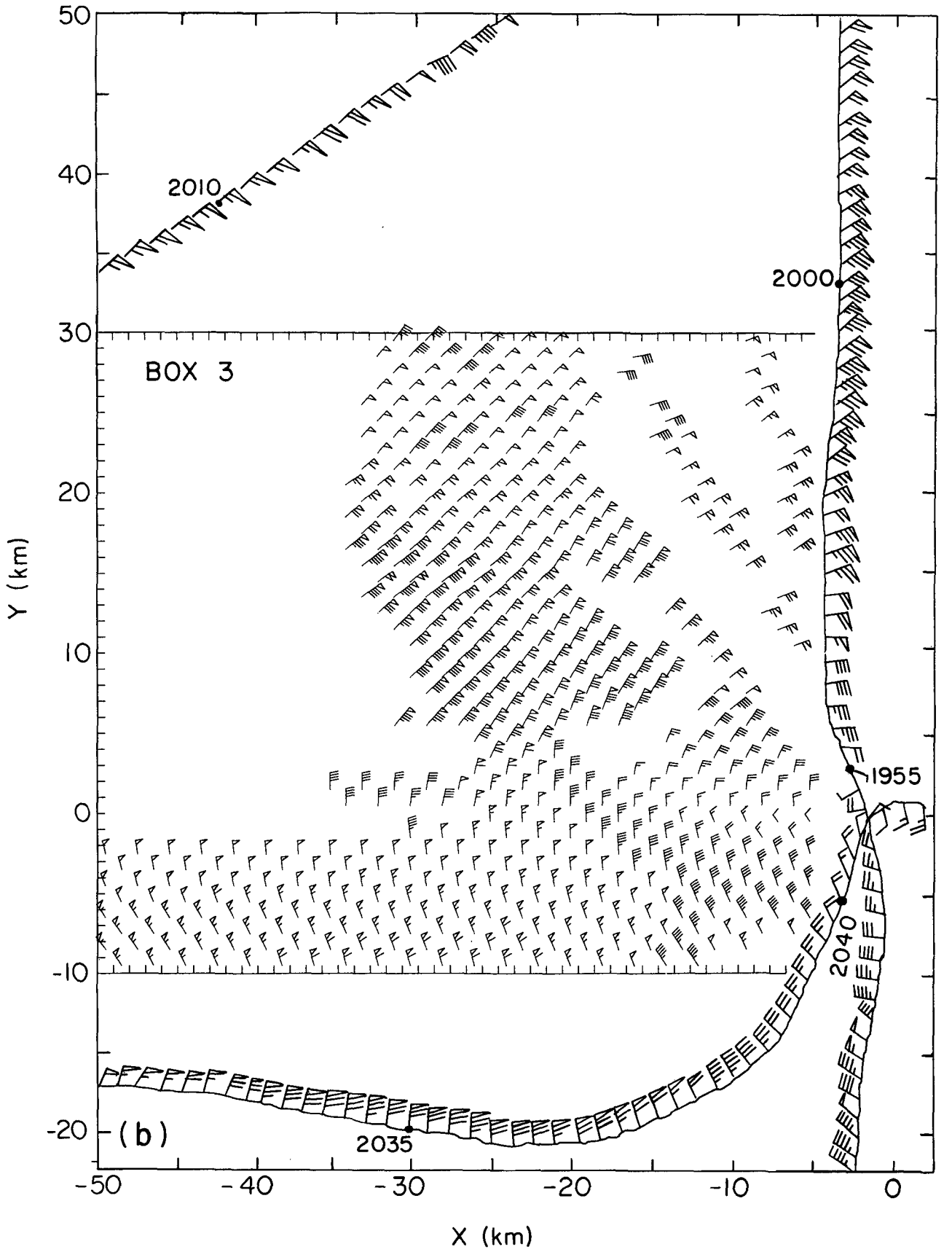

FIG. 2b. Doppler-derived winds in Box 3.

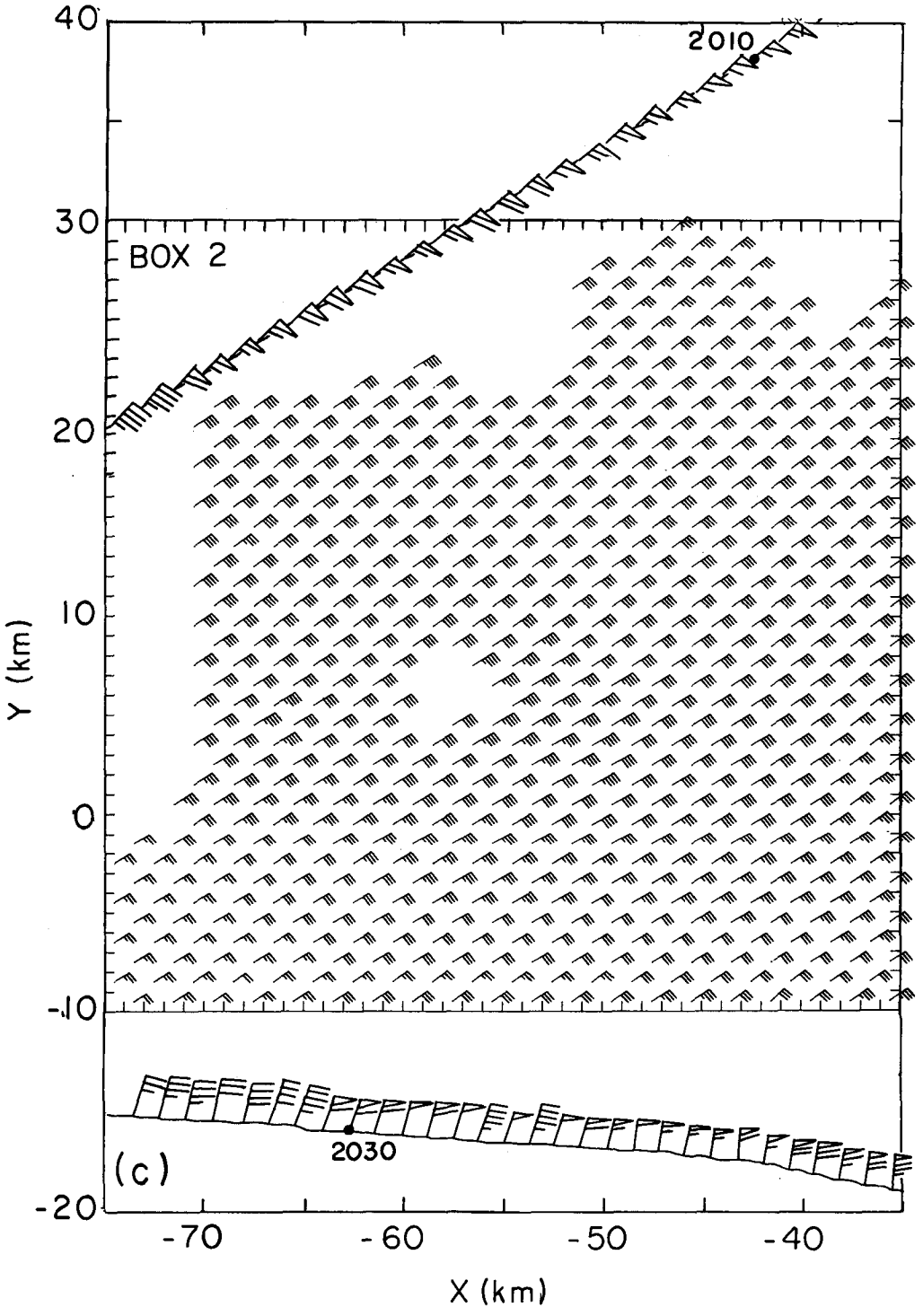

FIG. 2c. Doppler-derived winds in Box 2.

First, a minor discrepancy is seen in the extreme southeastern corner, where the speeds of the Doppler winds in Box 3 are greater than the speeds of the aircraft winds along the later (south-southwest to north-northeast) flight leg in that vicinity. The speeds of the Box 3 Doppler winds, however, were consistent with the earlier (south to north) flight leg in that region. The second discrepancy is noted where the Doppler winds in the southwestern portion of Box 3 (from X = −25 to −50 km and from Y = 0 to −10 km) are in sharp disagreement with the aircraft winds along the west-east flight track south of Box 3. These Doppler winds also disagree strongly with the Doppler winds in the southern part of Box 2 (Fig. 2c). The Doppler winds in the southern part of Box 2 also disagree with the aircraft winds to the south. These Box 2 winds are too easterly, however, in contrast to those in the southwestern part of Box 3, where the winds are too

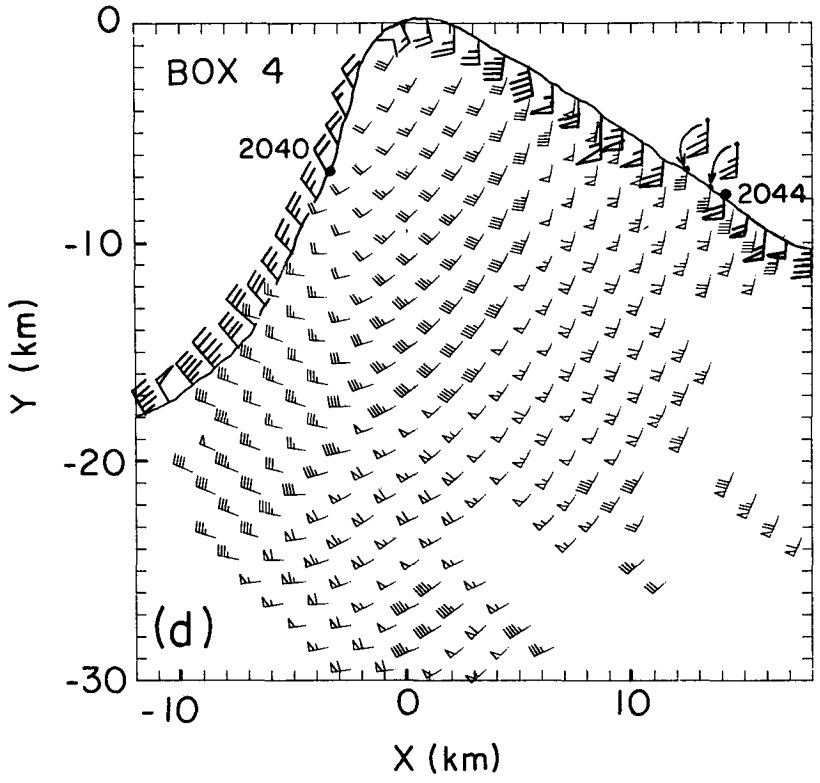

FIG. 2d. Doppler-derived winds in Box 4.

northerly. Because of the lack of agreement of the southwestern part of Box 3 and the southern part of Box 2, both with each other and with the aircraft winds, little confidence is placed in those regions of analysis.

An additional problem with Box 2 is noted in its northern portion, where the Doppler wind's speed disagrees with the aircraft winds along the flight track crossing the northwestern corner of the box.

An improved analysis in Box 2 and the southwestern part of Box 3 probably could be obtained by employing a method such as the overdetermined dual-Doppler technique described by Ray and Sangren (1983), in which the wind at any point is determined as a best fit to data from all available viewing positions, rather than from only two viewing angles at a time. Alternatively, the pseudo-dual Doppler technique of Jorgensen *et al.* (1983) could be refined to include explicit corrections for temporal differences, ground clutter, terminal fallspeeds, antenna biases, or other possible sources of error. For the present, however, conclusions may be drawn only from the more credible regions of analysis. The regions of credible winds covered most of the developing eye wall region, which was of primary interest in this study.

The Box 4 Doppler winds (Fig. 2d) are highly consistent in direction with the aircraft winds in that region. Some differences in speed are noted along the northeastern flight leg, where the Doppler winds are somewhat weaker than the aircraft winds. The primary use of the Box 4 winds was to construct streamlines in the southeastern quadrant of Debby. For this purpose, the accuracy of the winds was quite sufficient.

A further test of the quality of the low-level Doppler winds was accomplished by constructing streamlines of the storm circulation from a mosaic of the Doppler winds in Boxes 1, 3, and 4 (Fig. 2e). A well-defined circulation was obtained, with a center displaced from the origin of the X-Y coordinate system by only 3 km. Since the origin of the reference frame corresponds to the center of the storm determined as an objective fit to the 450 m level aircraft winds by the method of Willoughby and Chelmow (1982), the Doppler wind center near the origin attests to the overall consistency of the Doppler and aircraft winds. The Willoughby and Chelmow method of locating the storm center is expected to be accurate only to within a few kilometers. Therefore, the agreement we have obtained is as good as can be expected.

b. Winds at different altitudes

Doppler-derived winds in the overlap regions of Boxes 1 and 3 and Boxes 2 and 3 have been averaged level-by-level, and are compared in Fig. 3. Too few data were present in the overlap region of Boxes 1 and 2 for a similar comparison to be made for those two boxes.

In the Box 1–3 comparison (Fig. 3a), excellent agreement was found at all levels, with Box 3 showing only slightly greater wind speeds. This agreement lends further confidence to the Box 1 winds, which in Section 4a also were seen to have agreed well with the aircraft winds.

The Box 2–3 comparison (Fig. 3b) shows sharp disagreement at low levels (below 3 km) and upper levels (above 7

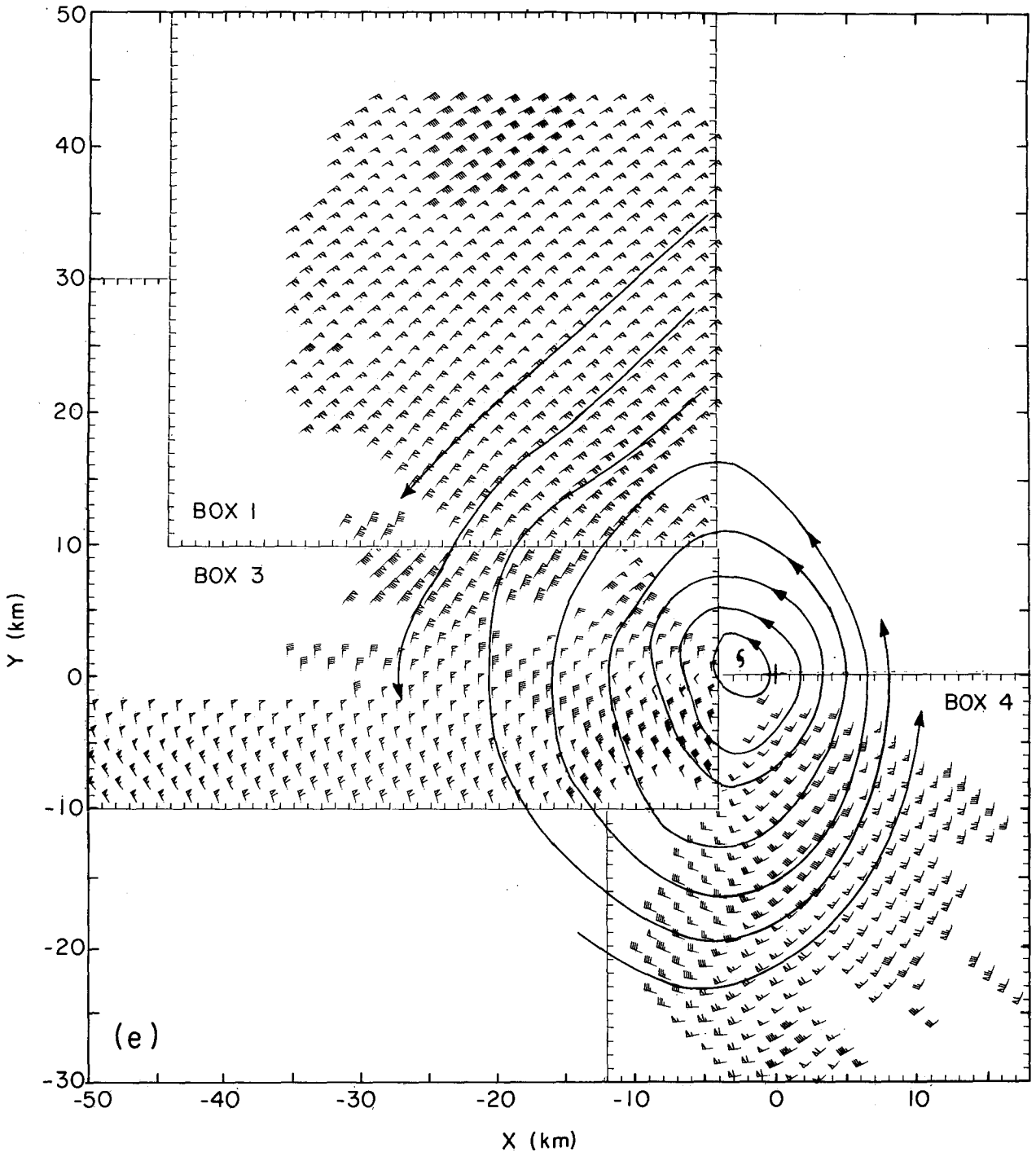

FIG. 2e. Mosaic of Doppler-derived winds in Boxes 1, 3, and 4, with streamlines and storm-center location implied by the streamlines of the Doppler winds also indicated.

km), with general agreement from 3 to 7 km. The agreement at middle levels suggests that the poor quality of the winds in the Box 2–3 overlap region noted in Section 4a might have been mainly a feature of the low- and upper-level flow, and that the mid-level winds might have been more reliable in these regions. Nevertheless, to be cautious, all Box 2 winds and the winds in the southwestern part of Box 3 in the analyses presented in the remainder of this paper have been disregarded.

5. Analysis of the Doppler-derived winds

The tail-radar reflectivity and wind analyses for the 1, 3, and 5 km levels are shown in Figs. 4–6. The wind analyses were constructed for altitudes up to 8 km. The winds above 5 km are not shown here because the region covered by echo decreased with height, and the areas in which Doppler-derived winds could be obtained decreased correspondingly.

Each of the panels in Figs. 4–6 has been constructed by

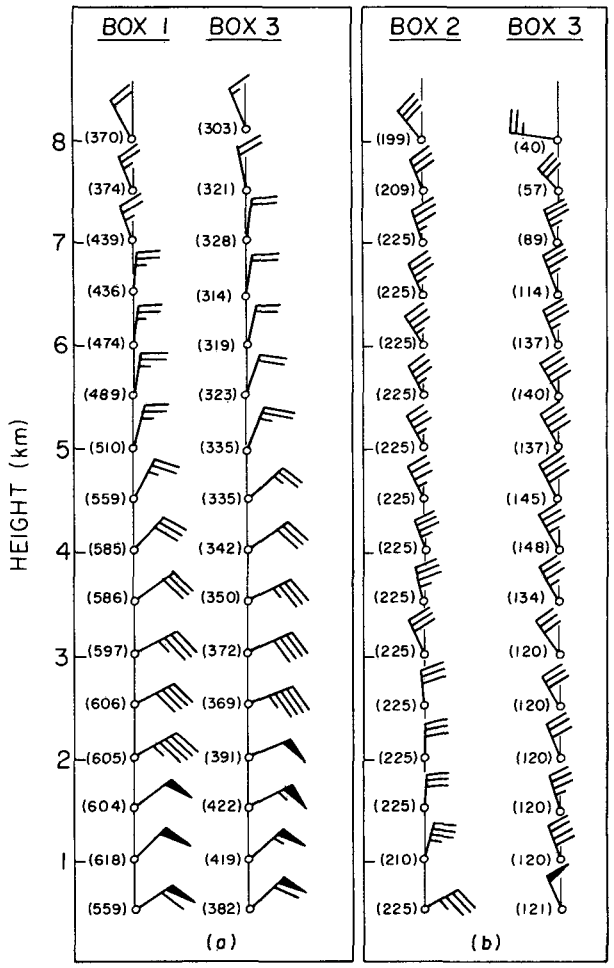

FIG. 3. Mean winds in overlap regions of a) Boxes 1 and 3 and b) Boxes 2 and 3 at various altitudes. Numbers in parentheses are areas (square kilometers) of overlap regions at each level.

combining the Box 1 analysis with the southeastern portion of the Box 3 analysis. The analysis shown south of Y = 10 km in each panel is from Box 3, while that north of Y = 10 km is from Box 1.

a. Reflectivity patterns

The radar reflectivity analyses in Figs. 4a, 5a, and 6a show that at 1 km the developing eye wall had a double structure. An outer band crossed Y = 10 km west of X = −30 km, while an inner band intersected Y = 10 km between X = −15 and −25 km. An offshoot of the inner band extended along Y = 0 between X = −7 and −27 km. The outher band generally was more intense and extended upward through the 3 and 5 km levels. The inner band sloped outward (from the storm center) and merged with the outer band at 5 km. A radially outward slope is a characteristic of well-developed eye walls of mature hurricanes (Jorgensen, 1984a,b), and here it may be an indication that the developing eye wall was beginning to take on the structure of a mature storm.

b. Wind fields

It was seen in Fig. 2e that at 0.5 km the flow around Debby constituted a well-defined storm circulation with no apparent superimposed structure. In contrast, the streamlines of the Doppler winds at the 1–5 km level (Figs. 4b, 5b, and 6b) show a distinct cyclonic perturbation superimposed on the circulation around the storm center. At 1 km (Fig. 4b), this perturbation was manifested as a sharp trough, with weak winds and a nearly closed circulation centered near X = −10 km, Y = 0 km. This position corresponded to the eastern end of the offshoot of echo from the inner band (seen in Figs. 4a and 5a). At 3 km (see Fig. 5b and cover photograph), the trough was broader and contained a closed mesocyclone centered at the western end of the echo offshoot seen in Figs. 4a and 5a. The line of confluence extending downwind of the mesocyclone center at 3 km coincided with the echo offshoot. At 5 km (Fig. 6b), the trough was broad north of its 3 km position (cf. Fig. 5b) and showed no closed center.

The existence of this sloping trough indicates that the flow around a developing hurricane can be highly disturbed on the mesoscale. To show that the mesocyclone (or subvortex) seen in Fig. 5b (and in the cover photograph) was really a circulation separate from the storm-scale vortex, we have constructed a streamline pattern for a mosaic of the 2.5 km level from Boxes 1, 3, and 4 (Fig. 7). This level was chosen because the mesocyclone was defined best at this height. The storm-scale vortex center can be seen at X = 0 km, Y = 0 km, while the mesocyclone is located at X = −20 km, Y = 4 km.

Suggestions of smaller-scale eddies embedded in the flow around a hurricane can sometimes be seen in cloud photography from satellites and high-flying aircraft (e.g., see picture on p. 102 of Fletcher *et al.*, 1961).[5] The airborne Doppler radar wind data, however, provide the first definitive documentation of such a feature.

Significant displacements between surface and aircraft-determined upper-level circulation centers of developing tropical cyclones have been reported by Huntley and Diercks (1981) and attributed by them to vertical tilt of the main

FIG. 4. (*Pages 578 and 579*) Analysis of reflectivity and wind fields at the 1 km level, derived from airborne Doppler radar data obtained in Hurricane Debby between 1950 and 2045 GMT, 14 September 1982. Coordinates are east-west distance (X) and north-south distance (Y) from the storm center. Each panel is a merger of the analysis from Box 1 north of Y = 10 km and Box 3 south of Y = 10 km. a) Reflectivity contours for 30 and 40 dB(Z). b) Wind analysis. Plotting convention same as in Fig. 2.

FIG. 5. (*Pages 578 and 579*) Same as Fig. 4, except for 3 km level.

FIG. 6. (*Pages 578 and 579*) Same as Fig. 4, except for 5 km level.

[5] This fact was pointed out to us by Peter G. Black, who also showed us an analysis of aircraft wind data indicating that a mesocyclone might have been present at the 6–7 km level, some 80 km from the low-level storm center, in the early stages of Hurricane Eloise of 1975.

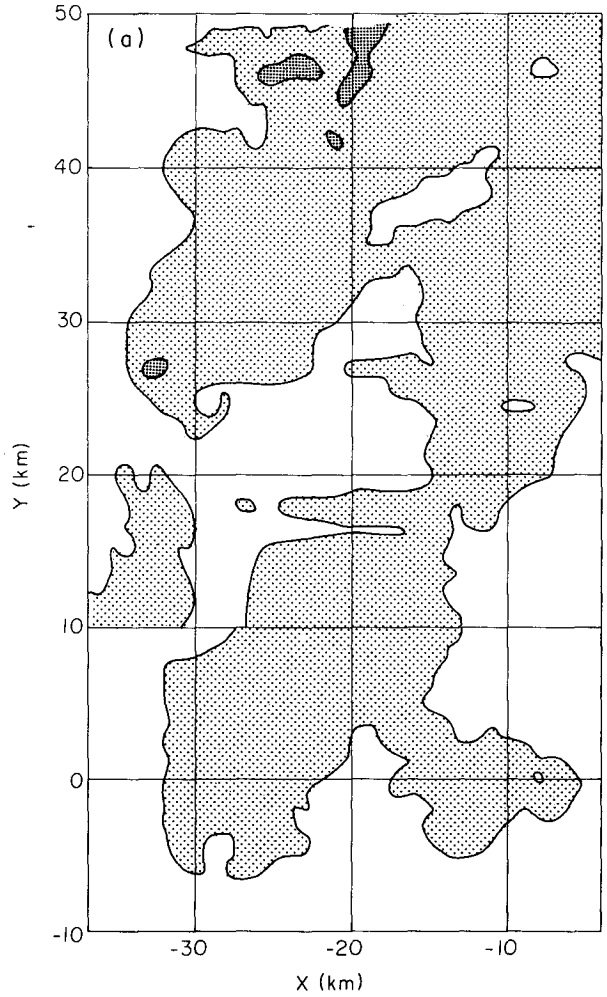

FIG. 4a. Reflectivity contours for 30 and 40 dB(Z).

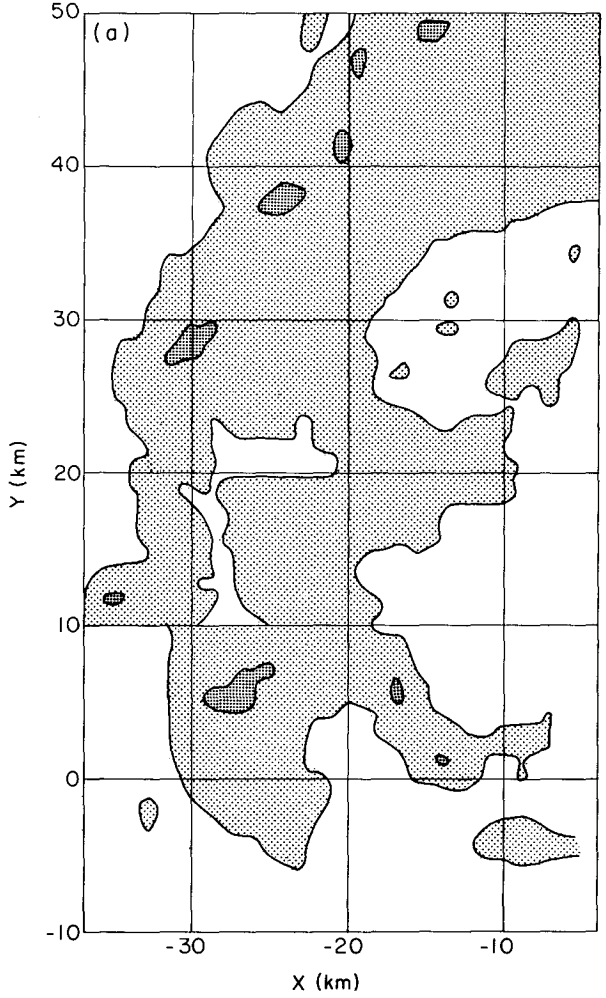

FIG. 5a. Same as Fig. 4a, except for 3 km level.

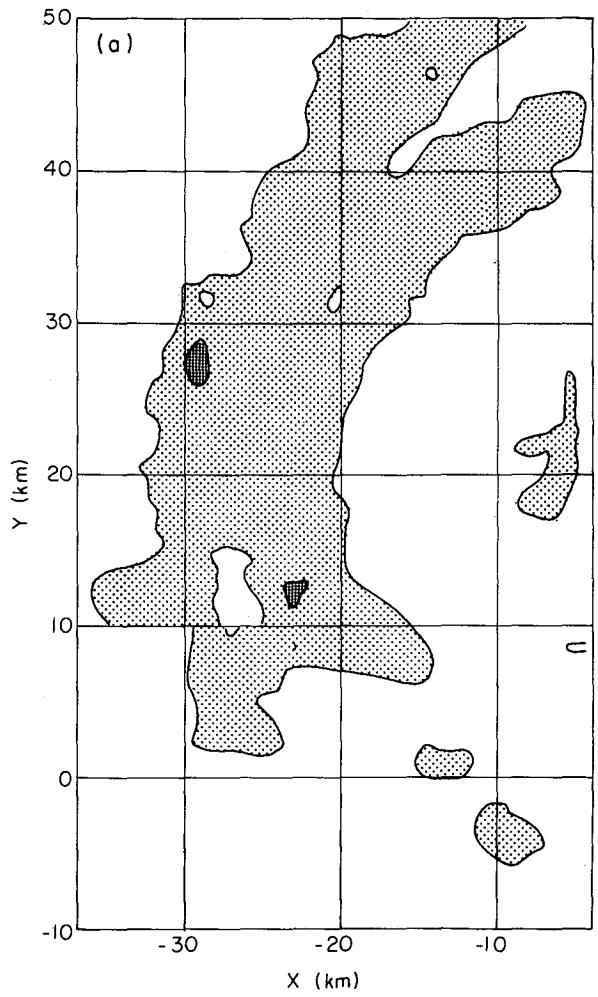

FIG. 6a. Same as Fig. 4a, except for 5 km level.

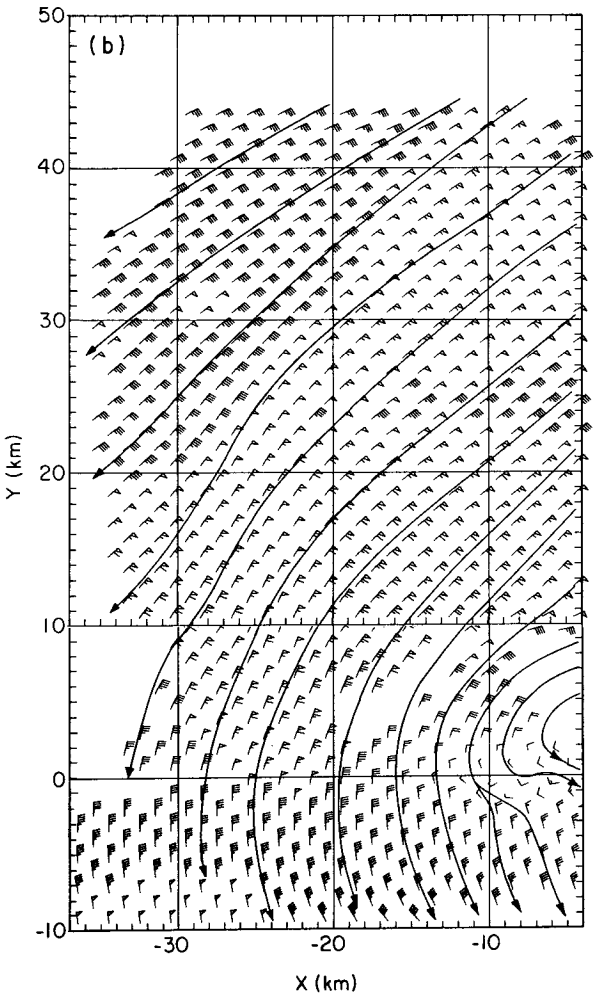

FIG. 4b. Wind analysis. Plotting convention same as in Fig. 2.

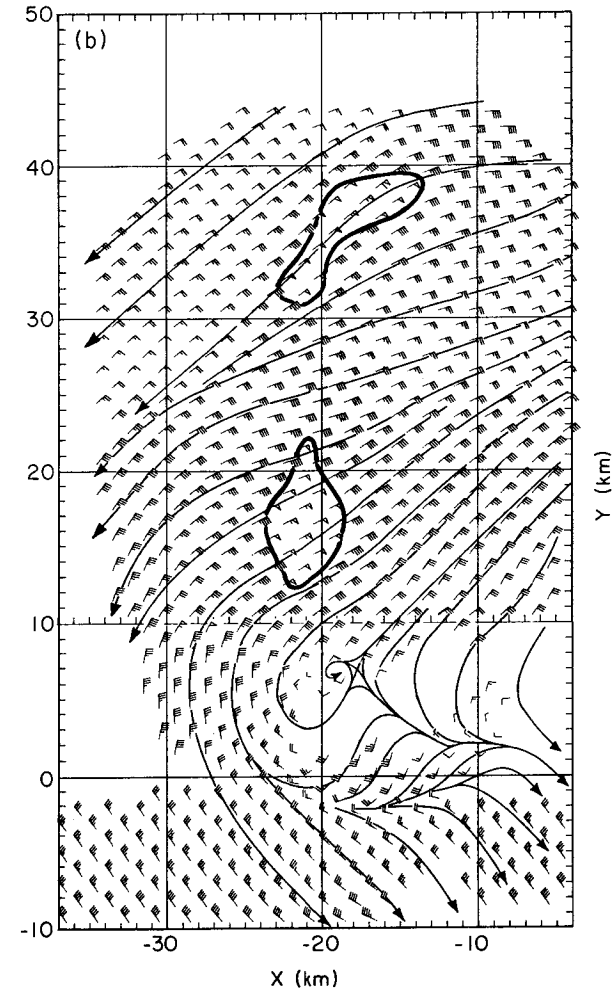

FIG. 5b. Same as Fig. 4b, except for 3 km level. Winds exceeding 23 $m \cdot s^{-1}$ are outlined by a heavy line.

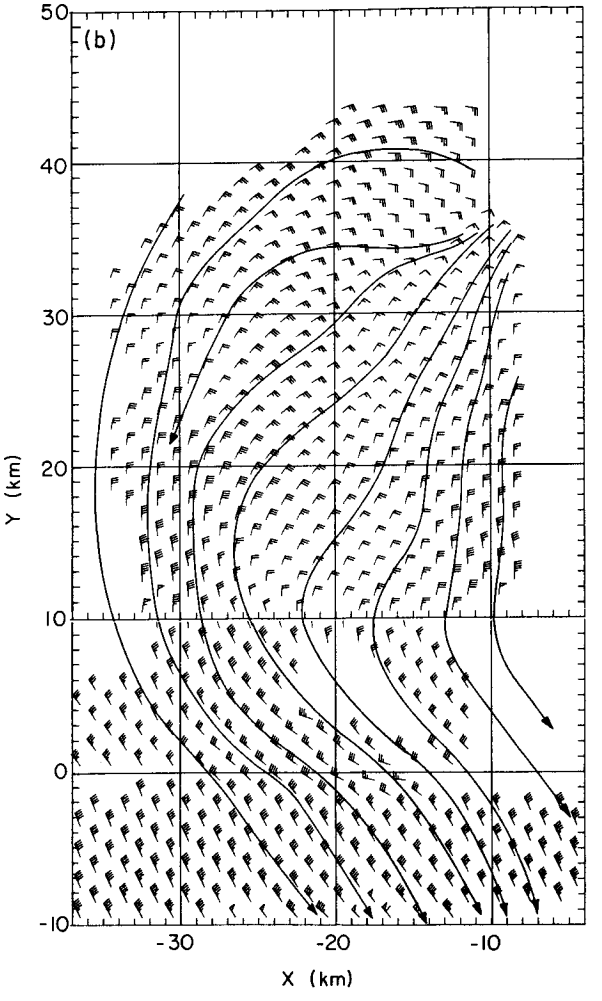

FIG. 6b. Same as Fig. 4b, except for 5 km level.

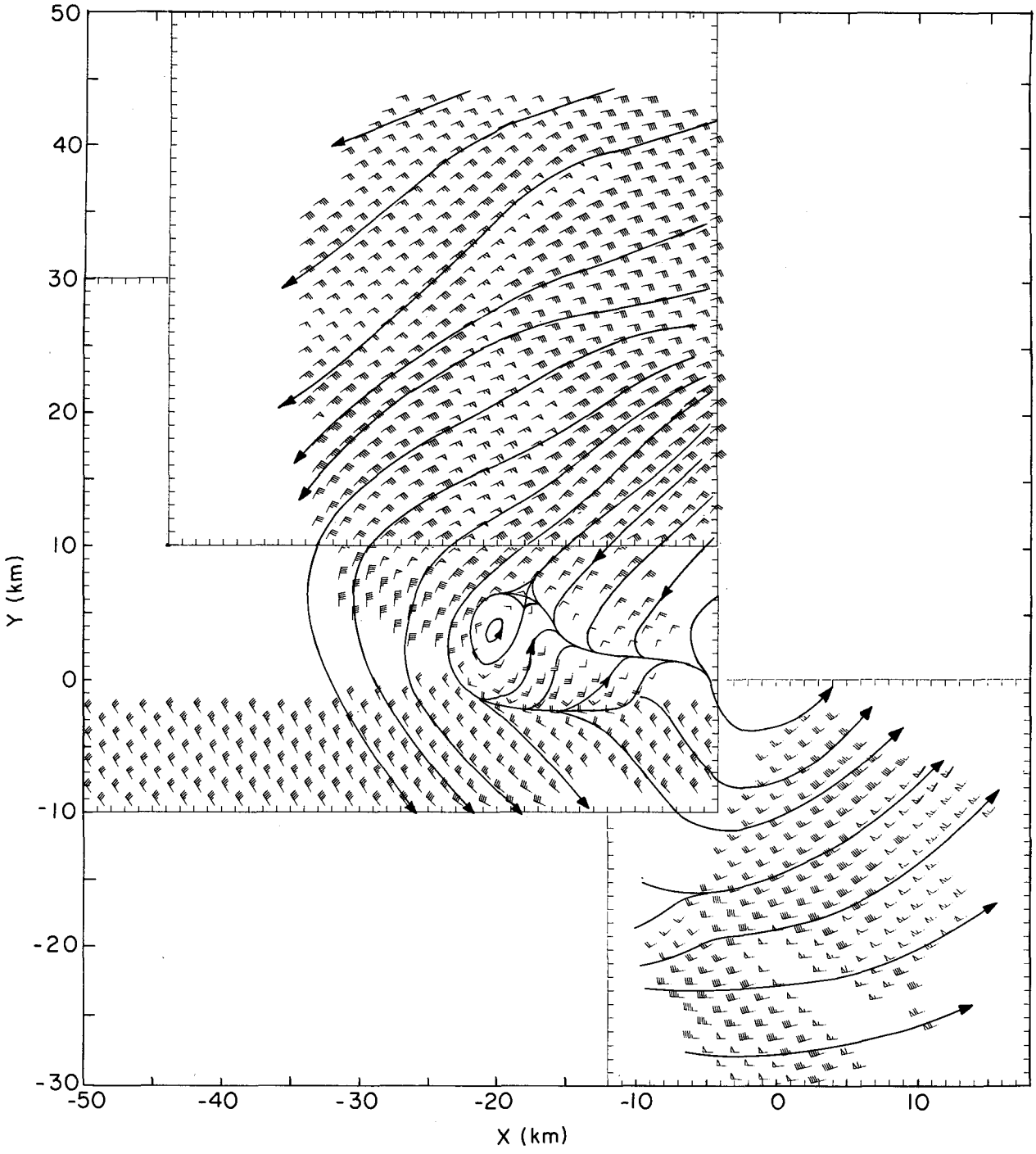

FIG. 7. Analysis of Doppler-derived winds at the 2.5 km level. The field is a mosaic of the wind patterns in Boxes 1, 3, and 4. Plotting convention same as in Fig. 2.

storm center. The airborne Doppler data suggest that such displacements may be indicated falsely by aircraft flight tracks through secondary vortex centers, such as the mesocyclone at the 3 km level in Debby. This secondary vortex center could be misinterpreted as the location of the main storm center at this level if a flight track happened to pass through it but not through the main storm center.

In addition to the mesocyclone, the flow at the 3 km level contained two other distinct mesoscale features. These were the wind maxima denoted by the closed isotachs seen at X = −19 km, Y = 37 km and X = −21 km, Y = 17 km in Fig. 5b. Mesoscale maxima also occurred at 1 and 5 km (isotachs not drawn in Figs. 4b and 6b), but showed no evident vertical continuity with those at 3 km.

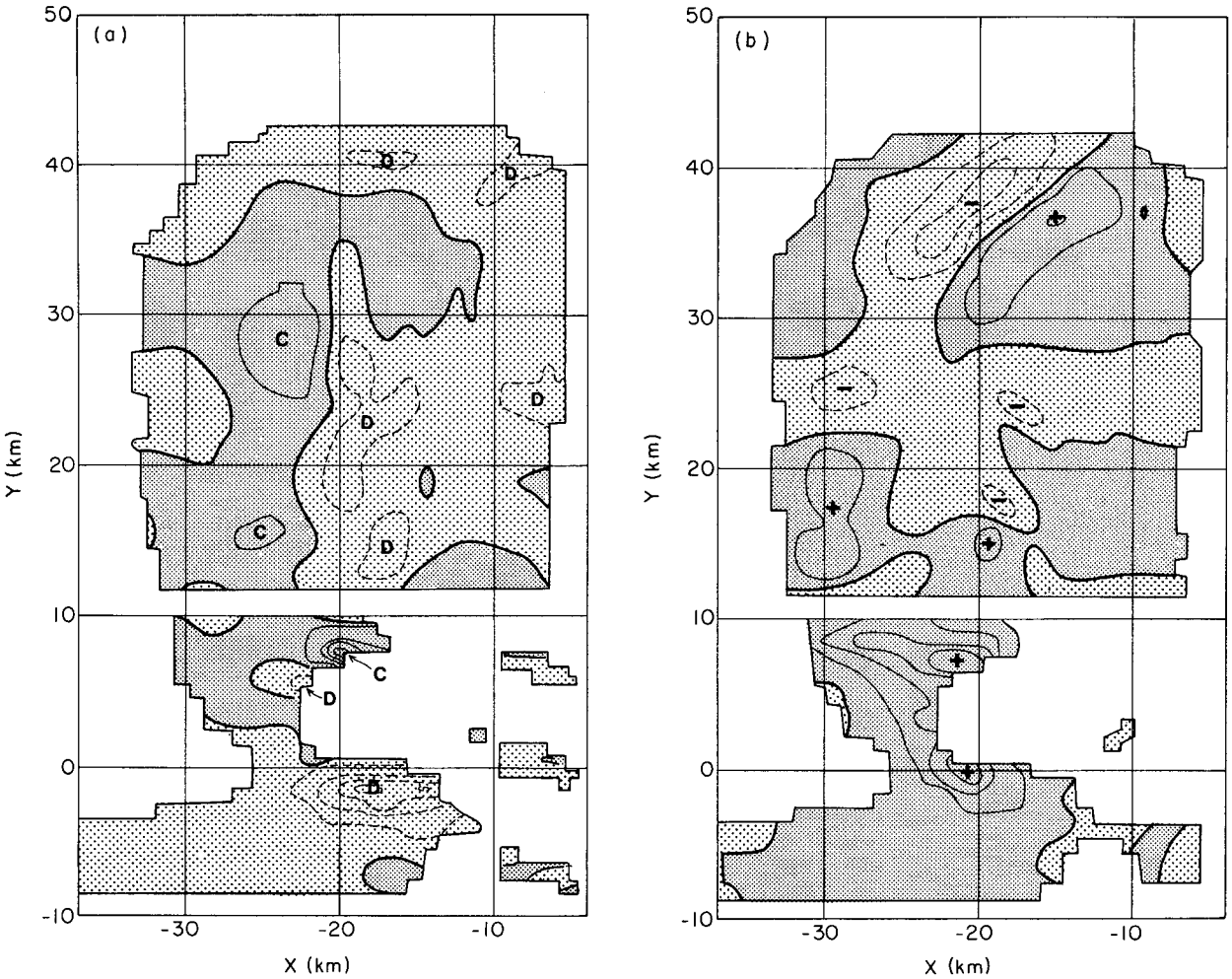

FIG. 8. a) Contours of divergence for values of -3, 0, 3, 4, 5, 6, 7, and 8×10^{-3} s. Zero line is heavy; positive contours are dashed; C and D indicate centers of convergence and divergence, respectively; regions where divergence calculations could not be made are left blank. b) Contours of relative vorticity for values of $-4, -2, 0, 2, 4, 6$ and 8×10^{-3} s. Zero line is heavy; negative contours are dashed; pluses and minuses indicate centers of positive and negative vorticity, respectively; regions where vorticity calculations could not be made are left blank. Coordinates are east-west distance (X) and north-south distance (Y) from the storm center. Each panel is a merger of the analysis from Box 1 north of Y = 10 km and Box 3 south of Y = 10 km.

c. Divergence and vorticity

The divergence of the Doppler-derived wind field at 3 km is shown in Fig. 8a. A band of convergence lay parallel to the large rainband seen in Fig. 5a. The convergence was concentrated in peaks associated with the three mesoscale features noted in the wind field, however. Maxima of convergence (at X = −24 km, Y = 27 km and X = −25 km, Y = 15 km) were just downwind of the two mesoscale wind speed maxima seen in Fig. 5b. A third and stronger maximum of convergence (only partially shown because of incomplete data coverage) is seen at X = −20 km, Y = 8 km, near the center of the mesocyclone.

Also seen in Fig. 8a are two mesoscale areas of concentrated divergence. One is located just east of the convergence band, radially inside the large rainband (along X = −17 km, between Y = 10 and 30 km). The other (centered at X = −17 km, Y = −2 km) is associated with the region of strong diffluence seen just south of the mesocyclone in Fig. 5b).

The relative vorticity field (Fig. 8b) also was dominated by the mesoscale features seen in the wind field. A strong vorticity couplet (centered at X = −17 km, Y = 37 km) was associated with the northern mesoscale wind maximum seen in Fig. 5b. This couplet lay just upwind of the northern convergence maximum seen in Fig. 8a. A weaker couplet was associated with the weaker wind maximum to the south (at X = −19 km, Y = 17 km in Fig. 5b). A major concentration of positive vorticity (centered at X = −20 km, Y = 7 km) was associated with the mesocyclone. Thus, the positive vorticity in the portion of the developing hurricane that we have examined was concentrated in patches associated with discrete mesoscale features of the circulation in the vicinity of the developing eye wall, especially near the mesocyclone.

6. Conclusions

The first use of airborne Doppler radar in the study of a hurricane has shown the data to be of good quality and has revealed mesoscale features of the storm circulation that have not been possible to document with flight-track data. In future studies, still better results may be obtained by refining the method of Jorgensen *et al.* (1983) to include explicit corrections for specific types of errors in the radar data or by adopting statistical techniques, such as the overdetermined dual-Doppler method described by Ray and Sangren (1983). By equipping more than one aircraft with Doppler radar, it will become possible to view the same point in space simultaneously from different viewing angles, thus eliminating the present inability to resolve highly transient features of the hurricane wind field. In coastal regions, it may be possible to coordinate airborne and land-based Doppler radar observations of hurricanes.

The airborne Doppler data show that the flow at the 3 km level in this particular region of the developing inner core of Hurricane Debby contained three distinct mesoscale disturbances. Two of these disturbances were evident as mesoscale maxima in the 3 km level windspeed field. Each of these speed maxima was characterized by a convergence maximum immediately downwind and a vorticity couplet straddling the speed maximum. These mesoscale wind maxima exhibited little vertical continuity.

The third mesoscale feature was a pronounced mesocyclone located along the southern part of the developing eye wall. This mesocyclone extended through the 1–5 km layer. It sloped northwestward with height (i.e., radially outward and tangentially upwind) and was associated with an intense subband in the precipitation pattern. The mesocyclone contained most of the positive vorticity of the flow in the developing eye wall region at the 3 km level. The positive vorticity in the mesocyclone at 3 km possibly was being advected toward the center of the storm by the large-scale, inwardly spiralling winds of the developing hurricane. Such advection may have influenced the evolution of the hurricane.

Future studies should be directed toward determining the frequency of occurrence of wind maxima, mesocyclones, and other mesoscale features embedded in the flows surrounding the inner cores of both developing and mature hurricanes. The dynamics of these features and their interactions with the storm-scale flow need to be understood. Airborne Doppler radar documentation of hurricane inner-core wind fields, together with parallel numerical modeling and theoretical efforts, should provide the means for tackling these problems over the next few years.

Acknowledgments. The data used in this study were gathered with the aid of the NOAA Office of Aircraft Operations flight crews and engineers, particularly Jim DuGranrut and Terry Schricker, who kept the airborne Doppler radar functioning during the 1982 hurricane season. David Jorgensen helped design the Doppler analysis software. We appreciate many helpful discussions with Peter Black, Stephen Lord, Lloyd Shapiro, and Hugh Willoughby. This research was supported partially by the National Science Foundation under Grant No. ATM 80-17327.

References

Bargen, D. W., and R. C. Brown, 1980: Interactive radar velocity unfolding. *Preprints, 19th Conference on Radar Meteorology (Miami Beach)*, AMS, Boston, pp. 278–283.

Barnes, G. M., E. J. Zipser, D. Jorgensen, and F. Marks, 1983: Mesoscale and convective structure of a hurricane rainband. *J. Atmos. Sci.*, **40**, 2125–2137.

Fletcher, R. D., J. R. Smith, and R. C. Bundgaard, 1961: Superior photographic reconnaissance of tropical cyclones. *Weatherwise*, **14**, 102–109.

Houze, R. A., Jr., S. G. Geotis, F. D. Marks, Jr., D. D. Churchill, and P. H. Herzegh, 1981: Comparisons of airborne and land-based radar measurements of precipitation during Winter MONEX. *J. Appl. Meteor.*, **20**, 772–783.

Huntley, J. E., and J. W. Diercks, 1981: The occurrence of vertical tilt in tropical cyclones. *Mon. Wea. Rev.*, **109**, 1689–1700.

Jorgensen, D. P., 1984a: Mesoscale and convective-scale characteristics of mature hurricanes. Part I: General observations by research aircraft. *J. Atmos. Sci.*, accepted for publication.

——, 1984b: Mesoscale and convective-scale characteristics of mature hurricanes. Part II. Inner core structure of Hurricane Allen (1980). *J. Atmos. Sci.*, accepted for publication.

——, P. H. Hildebrand, and C. L. Frush, 1983: Feasibility test of an airborne pulse-Doppler meteorological radar. *J. Climate Appl. Meteor.*, **22**, 744–757.

Ray, P. S., and K. L. Sangren, 1983: Multiple-Doppler radar network design. *J. Climate Appl. Meteor.*, **22**, 1444–1454.

——, R. J. Doviak, G. B. Walker, D. Sirmans, J. Carter, and B. Bumgarner, 1975: Dual-Doppler observation of a tornadic storm. *J. Appl. Meteor.*, **14**, 1521–1530.

Shapiro, L. J., and H. E. Willoughby, 1982: The response of balanced hurricanes to local sources of heat and momentum. *J. Atmos. Sci.*, **39**, 378–394.

Shea, D. J., and W. M. Gray, 1973: The hurricane's inner core region, symmetric and asymmetric structure. *J. Atmos. Sci.*, **30**, 1544–1564.

Trotter, B. L., R. C. Strauch, and C. L. Frush, 1981: Evaluation of a meteorological airborne pulse-Doppler radar. *NOAA Tech. Memo ERL WMPO-45*, Boulder, Colo., 55 pp. (NTIS No. ADA092276).

Willoughby, H. E., and M. B. Chelmow, 1982: Objective determination of hurricane tracks from aircraft observations. *Mon. Wea. Rev.*, **110**, 1298–1305.

——, J. A. Clos, and M. G. Shoreibah, 1982: Concentric eye walls, secondary wind maxima, and the evolution of the hurricane vortex. *J. Atmos. Sci.*, **39**, 395–411.

——, J. Han-Liang, S. J. Lord, and J. M. Piotrowicz, 1984: Hurricane structure and evolution as simulated by an axisymmetric, nonhydrostatic numerical model. *J. Atmos. Sci.*, accepted for publication.